New Journal of Physics
The open-access journal for physics

Nanoantenna array-induced fluorescence enhancement and reduced lifetimes

Reuben M Bakker[1], Vladimir P Drachev[1], Zhengtong Liu[1], Hsiao-Kuan Yuan[1], Rasmus H Pedersen[2], Alexandra Boltasseva[1,3], Jiji Chen[4], Joseph Irudayaraj[4], Alexander V Kildishev[1] and Vladimir M Shalaev[1,5]

[1] School of Electrical and Computer Engineering, Birck Nanotechnology Center, Purdue University, West Lafayette, IN 47907, USA
[2] MIC-Department of Micro and Nanotechnology, Technical University of Denmark (DTU), DK-2800 Kgs Lyngby, Denmark
[3] COM•DTU, Technical University of Denmark (DTU), DK-2800 Kgs Lyngby, Denmark
[4] Department of Agricultural and Biological Engineering and Bindley Biosciences Center, Purdue University, West Lafayette, IN 47907, USA
E-mail: shalaev@purdue.edu

New Journal of Physics **10** (2008) 125022 (16pp)
Received 21 May 2008
Published 16 December 2008
Online at http://www.njp.org/
doi:10.1088/1367-2630/10/12/125022

Abstract. Enhanced fluorescence is observed from dye molecules interacting with optical nanoantenna arrays. Elliptical gold dimers form individual nanoantennae with tunable plasmon resonances depending upon the geometry of the two particles and the size of the gap between them. A fluorescent dye, Rhodamine 800, is uniformly embedded in a dielectric host that coats the nanoantennae. The nanoantennae act to enhance the dye absorption. In turn, emission from the dye drives the plasmon resonance of the antennae; the nanoantennae act to enhance the fluorescence signal and change the angular distribution of emission. These effects depend upon the overlap of the plasmon resonance with the excitation wavelength and the fluorescence emission band. A decreased fluorescence lifetime is observed along with highly polarized emission that displays the characteristics of the nanoantenna's dipole mode. Being able to engineer the emission of the dye–nanoantenna system is important for future device applications in both bio-sensing and nanoscale optoelectronic integration.

[5] Author to whom any correspondence should be addressed.

Optical nanoantennae are metal nanostructures that can act as transducers for receiving or transmitting electromagnetic energy at subwavelength, nanoscale dimensions. In many senses, they are analogous to antennae built for other wavelength scales along the electromagnetic spectrum [1]. The wavelength-scaling properties of electromagnetism allow the simple dipole antenna to be scaled to subwavelength dimensions for the visible and near-infrared portion of the spectrum [2]. When properly engineered, these nanostructures can provide increased light extraction (or collection) from emitters (or detectors) such as molecules, quantum dots and wells or any photoactive material. These properties are desirable for applications in biological and chemical sensing and imaging. Chip-level integration of optoelectronic devices such as photodetectors and light emitters will benefit from nanoantennae, along with more general photovoltaic and ambient lighting devices.

Over the past several years, optical nanoantenna systems have become common in the literature; the focus tends to be on dimer [3]–[28] or single [29]–[40] metal nanoparticle systems. The antenna properties originate with the ability of metal nanoparticles to support localized surface plasmon resonances (LSPRs) at optical frequencies [41]. Incident photons cause the collective oscillation of conduction band electrons in the metal. The fundamental mode is dipolar in nature and causes electric field enhancement. When two similar particles are brought into a dimer configuration, the LSPRs can couple together, resulting in a red shift in the resonance wavelength [5]–[9] and a higher electric field enhancement in the gap between the particles [10]–[16]. Following the antenna analogy, this gap is often referred to as the feed-gap of the nanoantenna.

The proliferation of advanced patterning techniques over the past 10 years has led to many different methods to fabricate highly controlled, dimer-based nanoantenna systems. These techniques include nano-manipulation with an atomic force microscopy probe, self assembly and lithography using focused ion beams, electron beams or nanoimprinting. The shapes of the fabricated particles include spheres, cylinders, ellipses, triangles and rectangles. Once a sample is prepared, the LSPR and subsequent field enhancement can be studied as a function of antenna shape, size and feed-gap dimension. Antennae have been studied with either plane wave illumination or localized emitters exciting and interacting with the LSPR. Localized emitters have included quantum dots [11, 30, 33, 37], fluorescent dyes [13], [20]–[23], [31], [33]–[35], [38]–[40], and Raman-active molecules [26, 27]. Optoelectronic device integration has begun to take advantage of the dimer nanoantenna configuration. In terms of emitters, nanoantennae have been fabricated on the facet of laser diodes to help localize the emission to a subwavelength spot [12], whereas in terms of a detection device, a germanium detector has been built that uses a dimer nanoantenna to help capture radiation [28].

It was realized in the early 1980s [42, 43] that fluorescence enhancement of the molecules near a metal nanostructure is a result of the modification of the molecule excitation as well as the radiative and nonradiative decay rates. Both enhancement and quenching of the molecule can be observed from the same system by varying the distance between a molecule and a spherical particle [31, 32]. The result of these competing processes depends on several factors, including the original molecular properties (quantum yield, radiative and nonradiative decay rates). The result also differs for spheroids of different aspect ratios and for different relative positions of the plasmon resonance, the excitation wavelength and the emission band. Previous studies were mostly focused on single particles and to some extent considered isolated particle dimers. Particle pair arrays, however, are not as thoroughly studied and are the focus of this work. Theoretical studies [44, 45] show that while the enhancement of the radiative efficiency due to

an isolated particle is significant, only modest enhancement can be achieved with an ordered array. A random assembly holds an advantage over the ordered array [44, 45].

It has been demonstrated recently [23] that Au nanoantenna arrays coated with the fluorescent dye molecule Rhodamine 800 (Rh800) embedded in a matrix of tetraethoxysilane (TEOS) induce strong, wavelength-dependent fluorescence enhancement. Such a system was developed to control the plasmon resonance [14] and potentially can be applied for gain-mediated improvements in the quality of the plasmon resonance.

In this paper, fluorescence enhancement of a Rh800/TEOS film via optical nanoantennae is studied to gain insight into the enhancement origin. The experiments involve fluorescence lifetime and polarization anisotropy measurements in addition to absorption and fluorescence spectroscopy. Emission from the excited dye molecules couples with LSPR modes in the nanoantenna. The optical antenna acts to enhance both the excitation and the out-coupling of the near-field of the emitting molecules to the far-field, and it also acts to change the angular distribution of the emission. The resulting enhancement of the fluorescence signal observed in our experiments varies as a function of wavelength for different antenna geometries and ranges from a factor of 10 to a factor of 70. As the antenna gap is decreased, the enhanced fluorescence (EF) signal increases. In part, the observed fluorescence enhancement is a result of the enhanced absorption at the excitation wavelength, giving a factor of about 1.5–1.7 on average over the dye film volume. A noticeable effect on the directionality of the emission has been observed by varying the acceptance angle of collection objectives with the same magnification. An estimate for a hemisphere-averaged enhancement leads to a lower bound for the quantum yield enhancement of about 2. The quantum yield, Q, for Rh800 in a TEOS matrix is measured to be about 0.03, which is much lower than the value in ethanol (0.21). The fluorescence lifetime τ measurements show that the excitation of the dye interacting with the nanoantenna decays at a rate three times faster than dye away from the nanoantenna. This lifetime decrease is mainly due to the three-times-higher nonradiative decay rate γ_{nr}. Consequently, the radiative decay rate $\Gamma_{\mathrm{r}} = Q/\tau$ is increased by factor of about 6. The EF is highly polarized along the primary antenna axis, giving an indication of the primary plasmon mode and the antenna-induced out-coupling to far-field radiation modes.

Periodic nanoantenna arrays of several different elliptical geometries were fabricated on a quartz substrate. Spincoating was used to coat the substrate with a photoresist (ZEP520A), and a 20 nm layer of aluminum was deposited on top of it for conductivity purposes. Nanoantenna patterns were written using electron beam lithography (JEOL JBX-9300FS). After patterning, the aluminum layer was removed and the resist was developed. Then, a 40 nm layer of gold was deposited in a vacuum chamber. Finally, a liftoff technique produced gold ellipses in the desired pattern on the quartz substrate [14, 23].

Five different antenna geometries in large ($150 \times 150\,\mu$m) arrays are presented herein with plasmon resonances close to the Rh800 excitation wavelength and emission band. Field-emission scanning electron microscope (FESEM) images of each geometry are presented in figure 1(a) along with their measured dimensions (ellipse length, ellipse width, gap, Y period and X period). Two closely spaced ellipses form one nanoantenna, which are periodically patterned in the X- and Y-directions.

Far-field transmission and reflection spectroscopy with linearly polarized plane wave illumination is used as a tool to characterize the LSPR modes. For light polarized along the primary nanoantenna axis, across the gap (X-direction), a strong resonance is seen in the red portion of the spectrum (figure 1(c)). Light polarized in the Y-direction shows a much weaker

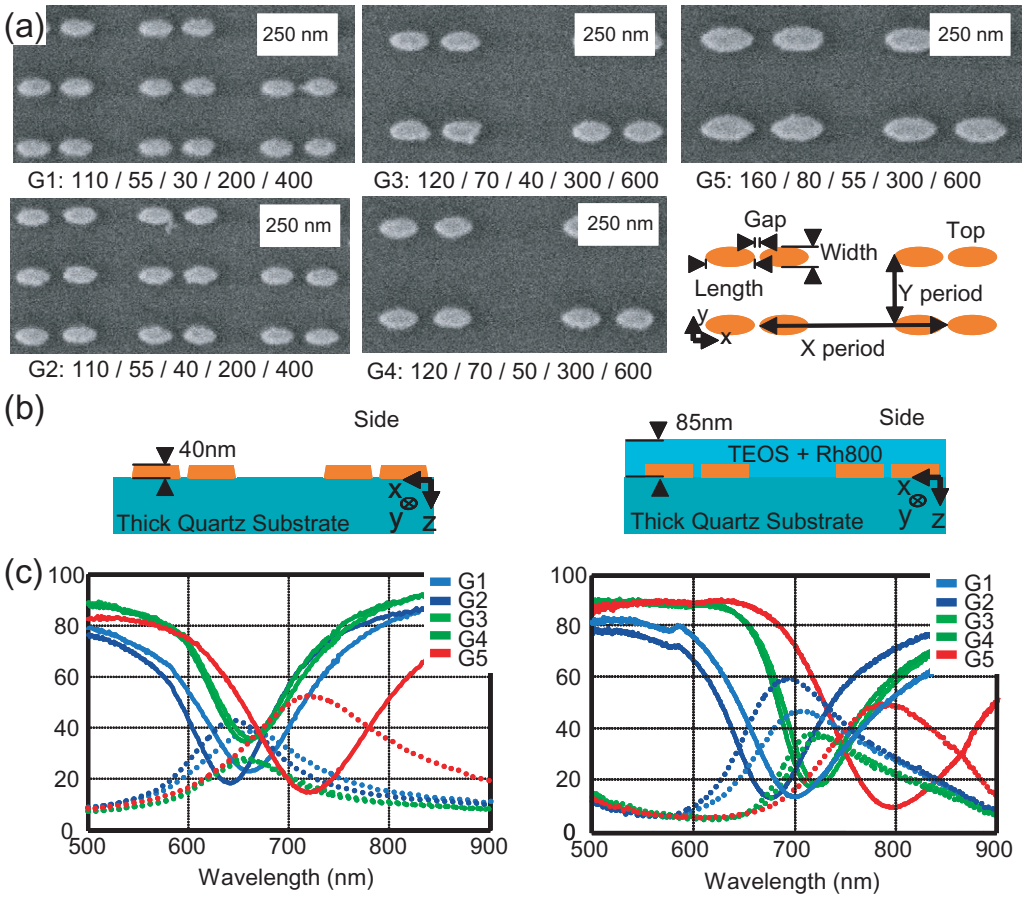

Figure 1. Nanoantenna sample showing five different geometries. (a) FESEM images of geometries 1, 2, 3, 4 and 5 along with an *XY* schematic of the array geometry. Dimensions in nanometers are below each picture (length/width/gap/*Y* period/*X* period). (b) Side view schematic of geometry before (left) and after (right) coating with a dielectric. (c) Far-field spectra for the five geometries before coating with a dielectric thin film (left) and after coating (right); the solid lines represent percent transmission and the dotted lines represent percent reflection for *X*-polarized light.

resonance in the green (not shown) [14]. Each geometry shows a distinct resonance due to the ellipse shape and gap. Geometry one (G1) and two (G2) have similar ellipse shapes, though G1 has a smaller gap that leads to increased plasmon coupling. In the far-field spectra, this increased coupling is seen via a 20 nm red-shift in the resonance wavelength of G1 compared with G2. A similar comparison can be made between G3 and G4, with G3 having a smaller gap that exhibits a 10 nm red-shift in resonance compared with G4.

Given the spectral range of the LSPRs and the predicted red-shift arising from coating the sample with a dielectric thin film, the fluorescent dye Rh800 was chosen so that the dye emission overlaps with the shifted LSPRs. TEOS was used as the host dielectric to place Rh800 molecules around the nanoantennae. A solution of TEOS, ethanol, water and hydrochloric acid (0.1 ml) at a molar ratio of 1 : 4 : 3 were mixed for 3 h. Then, Rh800 powder was mixed into the solution for 8 h. Spincoating was used to cover the nanoantenna sample with the dye-doped solution.

The sample was then baked at 60 °C for 8 h. Reactive ion etching (Plasmalab) was used to back etch the dielectric layer to a final thickness of 85 nm. The resultant concentration of Rh800 for the presented sample is 4.8 mM; this corresponds to ∼2.9 molecules in a 10 × 10 × 10 nm cube (∼2 × 10^4 molecules per dimer unit cell for G1/G2 and ∼4.4 × 10^4 molecules per dimer for G3, G4 and G5). A schematic of the sample with the dielectric coating is found in figure 1(b) (this recipe was first introduced in [23]). Far-field broadband spectroscopy for *X*-polarized light is shown in figure 1(c). As expected, each antenna array shows a red-shift in resonance due to the higher dielectric constant of TEOS compared with air. Rh800 has a quantum yield in ethanol of about 0.21 [46]. A comparative standard method [47] was used to measure Rh800 in TEOS relative to Rh800 in an ethanol solution placed in a 1 mm cuvette. A quantum yield of about 0.03 was determined, taking into account the ratio of the absorption, fluorescence signal, refractive index, and the slightly different ratio in the collection volume for absorption and fluorescence.

Figure 2(a) shows the far-field absorption spectra of the five different antenna geometries covered with TEOS compared with the emission and absorption spectra of Rh800 in TEOS. The Rh800/TEOS absorption spectrum was measured for a 400 nm film and then recalculated to the 85 nm case. The scale for the Rh800/TEOS is 30 times lower, meaning that the absorption maximum at 700 nm is about 1%. The spectral overlap between the plasmon resonances and the Rh800 absorption and emission varies for each antenna array. Figure 2(b) shows the results of the far-field photoluminescence measurements performed using a Renishaw inVia spectrometer. The spectrometer is fiber-coupled to an upright microscope, and the measurements were taken in a reflection configuration. Unpolarized 633 nm light was used to excite the Rh800 through an objective lens (50× magnification with a 0.45 NA). This pumping light overlaps with an absorption peak of Rh800, while its overlap with the nanoantenna absorption varies for each geometry. The emission of Rh800 also overlaps with and thus excites the primary antenna resonance. The end result is an EF signal from the antenna geometries. Light is collected with the same lens used for excitation. A long-pass filter blocks the excitation wavelength, and an optical fiber carries the fluorescence signal to the spectrometer.

Figure 2(b) shows the EF signal for the five antenna geometries compared with a Rh800 reference fluorescence signal taken on the same sample but away from the antenna arrays. These measurements were obtained with a weak irradiance (∼90 mW cm^{-2}) that is well below saturation of the dye transitions.

The enhancement factor is plotted in figure 2(c). It varies as a function of wavelength and is defined as $(I_{EF}(\lambda) - I_b(\lambda))/(I_F(\lambda) - I_b(\lambda))$ with $I_{EF}(\lambda)$ being the antenna-EF intensity; $I_F(\lambda)$ is the reference fluorescence signal and $I_b(\lambda)$ is the instrument background signal. The enhancement factors for all five geometries show a dip around 700 nm in the wavelength dependence. Rh800 in TEOS has a strong absorption peak around this wavelength range (see figure 2(a)). This dip indicates that the quality of the plasmon resonance at the emission wavelength is reduced in the absorptive host with enhanced absorption from the dye. This represents the feedback between the dye and the nanoantennae.

In examining the EF signals in figure 2(b), it is observed that the spectral shape and intensity are different for each geometry as the dye interacts differently with the distinct plasmon resonances. The EF can be compared as a function of gap size or ellipse shape. As a function of antenna gap, G1 should be compared with G2 and G3 with G4. In both of these comparisons, the antennae with the smaller gaps (G1 and G3) show a higher level of EF compared to the same ellipse geometries with a larger gap. The smaller antenna gap leads to increased plasmon coupling in the nanoantenna, a higher localized electric field and thus an increased extinction

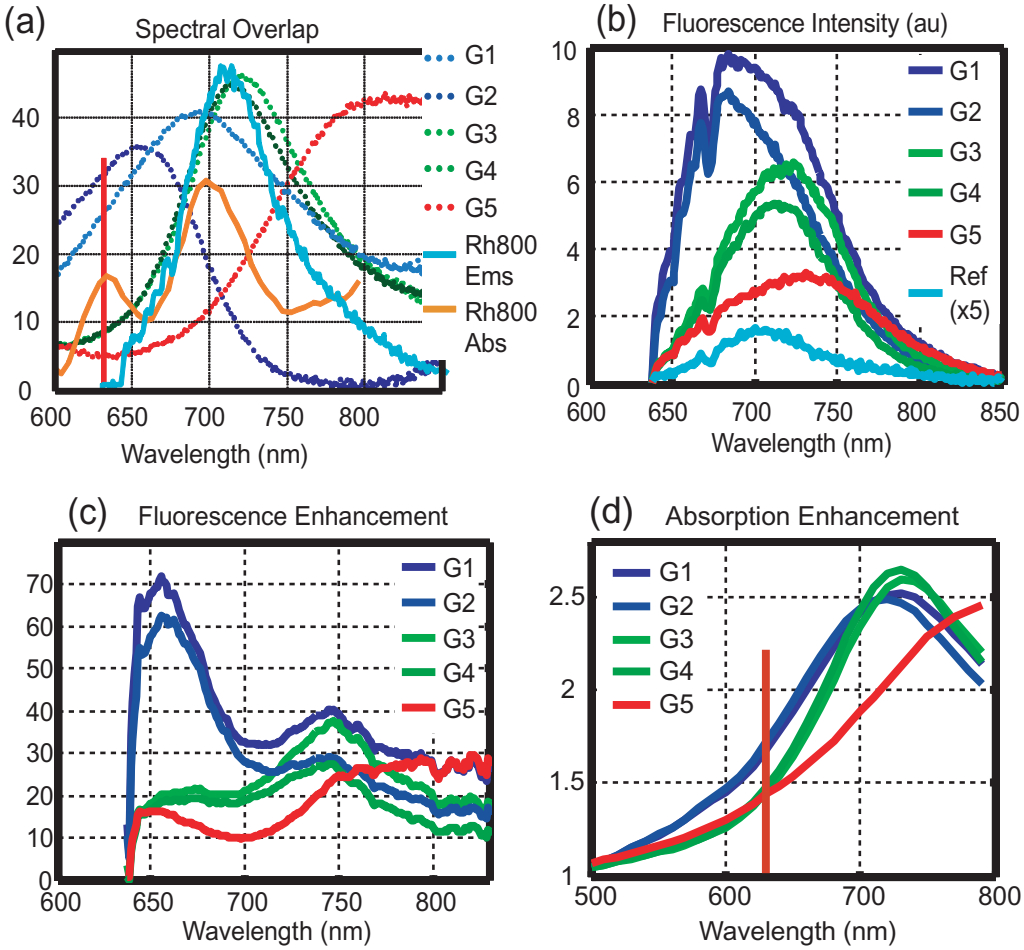

Figure 2. Enhanced fluorescence spectra. (a) Plasmon resonance spectra of nanoantennae (absorption) for the five geometries compared with a reference Rh800 emission spectrum in TEOS and a Rh800 absorption spectrum in TEOS times 30; the vertical line indicates the excitation wavelength of 633 nm (Y scale is only for the absorption). (b) Plasmon-EF as a function of wavelength compared with a reference Rh800 emission spectrum in TEOS. Note: the dip in the fluorescence spectra at 672 nm is due to a filter in the collection path. (c) Fluorescence enhancement factor as a function of wavelength. (d) Enhancement of the absorption in the Rh800/TEOS layer.

rate enhancement factor. The general shape of each EF spectrum can be thought of as a multiplication of the reference Rh800 emission and the antenna's LSPR spectrum. In comparing G1/G2, G3/G4 and G5, three distinct shapes are seen in the EF spectra. This is because the spectral overlap of Rh800 emission and the plasmon resonances are different for each geometry.

In order to separate the two contributions to the fluorescence enhancement factor, one from the excitation rate and the other from emission, numerical simulations of the absorption enhancement for the dye layer were performed. This was necessary because the dye absorption is masked by the nanoantennae in the experimental case. The simulation model was tested, and good agreement for the transmission and reflection spectra has been obtained. The results in

figure 2(d) show that the absorption enhancement varies from 1.5 to 1.7 at 633 nm for different arrays.

The antenna and dye emission coupling can strongly change the angular distribution of photoluminescence, which can lead to an increase in the amount of light propagating toward and collected by a detector in the far-field [39]. Measurements to test this possibility were performed with another objective that has the same magnification ($\times 50$) but an increased numerical aperture, NA $= 0.7$ instead of 0.45 as in the previous case. The enhancement factor for the fluorescence signal is decreased by factor of 1.5 using the new objective, indicating that the antenna strongly affects the angular distribution of the emission. This observation is important in understanding the antenna–dye system and will be further discussed below.

We considered the EF in more detail by performing lifetime and polarization experiments along with intensity distribution simulations. Simulations were used to examine the enhanced electromagnetic fields around the nanoantenna geometry. They show how the enhanced fields change as a function of the antenna feed gap. Fluorescence lifetime measurements indicate that the antenna interactions with the dye reduce the fluorescence lifetime of emitting molecules. Polarization measurements show that the EF is highly polarized and is characteristic of the dipolar plasmon mode of the nanoantenna. This result points toward a strong antenna effect where the antenna helps convert the near-field fluorescence into far-field propagating modes and thus significantly affects their basic properties. This is in agreement with recent observations for a single monopole antenna [39].

A commercial package (COMSOL) utilizing the three-dimensional finite element method in the frequency domain was applied to model the interaction of light with the nanoantenna arrays. Due to the symmetry of the design, a simulation space containing one quarter of the paired ellipse geometry was considered with perfectly matched layers at the top and bottom (Z-direction), perfect electrical conductors for the X boundaries and perfect magnetic conductors for the Y boundaries to emulate a large array. The simulation space was excited via plane wave illumination from above. A more detailed description of the simulations was reported in [14].

Electric field intensity mappings were created by sampling the near-field region of the simulation space excited by X-polarized light. Field mappings are presented for XY and XZ cross-sections in figures 3(b)–(d) for the ellipse shape of G1/G2 with three different gap sizes (20 nm, 30 nm and 40 nm). The mappings are averaged (XY in volume and wavelength, XZ in wavelength) to give some relationship to the effects seen by a fluorophore around the antennae. The averaging volume is demonstrated in figure 3(a) with a thickness of 90 nm above the substrate; this is similar to the 85 nm TEOS thickness of the real sample. The mappings are averaged over a 50 nm spectral width around the peak resonance wavelength. Though these mappings were created without a dielectric coating on top of the substrate, the effects and trends demonstrated are the same as if there were a dielectric coating in the simulation.

The mappings in figures 3(b)–(d) show the dipolar nature of the plasmon mode, with the highest electric field intensities at the ends of each ellipse. As the distance between the two ellipses decreases, the field intensity inside the gap increases along with the average intensity over the volume containing the dye.

In correlation with the enhanced electromagnetic fields afforded by the nanoantenna, the interactions between the localized emitters and the gold nanoantennae lead to a reduction in the excited state lifetime for the fluorophore. Fluorescence lifetime imaging microscopy (FLIM) was used to measure the fluorescence decay times of the presented nanoantenna

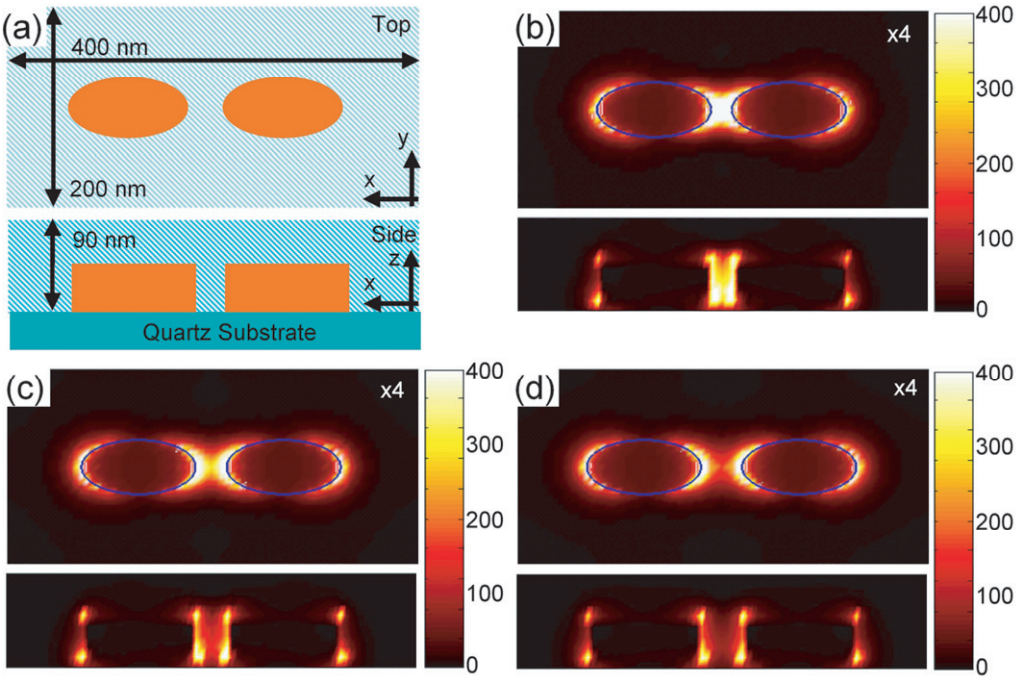

Figure 3. Electric field intensity maps from finite-element calculations for G1/G2 with various antenna gaps before coating with the dielectric film. (a) Schematic showing top and side views of a unit cell, the shaded area represents the volume where the dye would be. (b)–(d) *XY* mappings (top, corresponding to color bar scaled by a factor of 4) and *XZ* mappings (bottom, corresponding to color bar without scaling). (b) 20 nm gap; top view (*XY*) is averaged over 50 nm in spectral width and 90 nm above the substrate, the blue ovals mark the position of the ellipses; side view (*XZ* through the gap) is averaged over 50 nm in spectral width and shown for 90 nm above the substrate. (c) Same as (b) but with a 30 nm gap. (d) Same as (b) but with a 40 nm gap.

samples. FLIM measurements were performed using a confocal, time-resolved microscope on an inverted platform (MicroTime 200, PicoQuant GmbH [48]). A pulsed ($<$90 ps) 635 nm diode laser operating at 40 MHz was used to excite the sample through an objective lens (100$\times$ magnification, 0.75 NA). Light was collected through the same objective lens and an avalanche photodiode counted the photons in the fluorescence signal. Fluorescence intensity was measured as a function of time while the sample was raster scanned through the laser spot.

A characteristic lifetime measurement of an isolated nanoantenna (G4) is illustrated in figure 4. This single nanoantenna is $\sim$3.5 μm away from its nearest neighbor (diagonal direction). Figure 4(a) shows the fluorescence intensity as a function of position around the isolated antenna. Two regions are identified, an EF region coming from the antenna ($\sim$500 nm in diameter) and a reference region outside the EF region. The EF intensity is approximately three times greater than that of the reference region.

Two lifetime fittings were performed, the first one separately fitted each pixel in the measurement (figures 4(b) and (c)) while the second fitting (figure 4(d)) was cumulative and was used to fit the EF and reference regions separately. Figure 4(b) shows a mapping of the

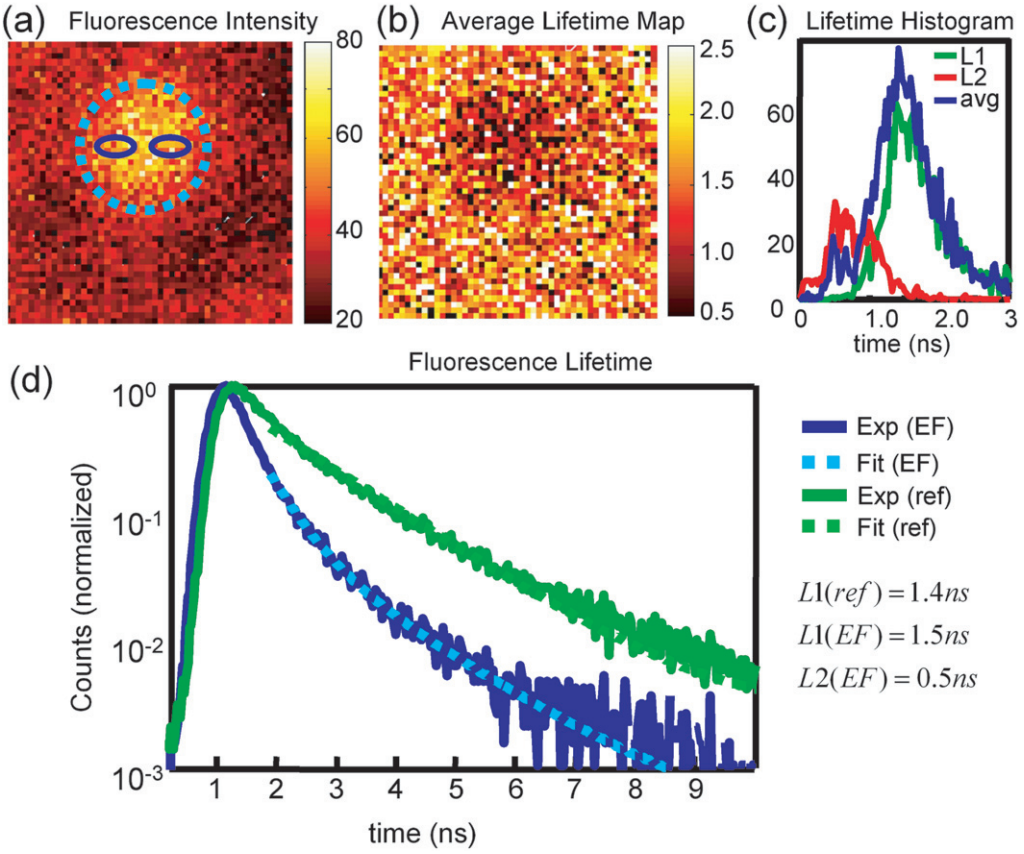

Figure 4. Fluorescence lifetime measurements on an isolated single nanoantenna (G4). (a) Fluorescence intensity around an isolated antenna; the solid ovals estimate the position of the nanoantenna particles, and the dotted circle is the boundary between EF and reference regions used in part (d). (b) Average fluorescence lifetime map (in ns) around an isolated antenna. (c) Fluorescence lifetime histogram corresponding to (b). (d) Normalized fluorescence decay comparing Rh800 interacting with the antenna to Rh800 away from an antenna (semilog). The reference signal, away from the antenna, is fitted with a single exponential decay ($L1 = 1.4$ ns) while the region interacting with the antenna is fitted with a double exponential decay ($L1 = 1.5$ ns and $L2 = 0.5$ ns).

average fluorescence lifetime for each pixel in the image. The region corresponding to the increased fluorescence signal in figure 4(a) shows a lower average lifetime than the region with background fluorescence. A histogram of the individually fitted lifetimes is plotted in figure 4(c) and shows a bimodal distribution; there is one peak at a shorter lifetime corresponding to interactions with the gold nanoantenna and a second peak corresponding to the adjacent regions with background fluorescence.

For the second, cumulative lifetime fitting, the measurement is divided into two regions: the EF region inside the dotted line of figure 4(a) and the reference (ref) region outside the dotted line. Fluorescence intensity is plotted as a function of time (semilog) for both regions in figure 4(d). The fluorescence interacting with the nanoantenna shows a decreased lifetime

compared with the reference signal. The reference signal is fitted with a single exponential decay (a lifetime of 1.4 ns) while the EF signal requires a double exponential decay to give a reasonable fit ($L1 = 1.5$ ns and $L2 = 0.5$ ns).

The lifetime values of the double exponential fit indicate that some of the dye interacts with the nanoantenna, leading to a reduced lifetime, whereas another portion of the dye does not interact much with the nanoantenna and decays at roughly the same rate as the reference fluorescence. The antenna interactions result in a 3-fold increase in the decay rate. Fluorescence lifetime measurements were also performed on G4 in a regularly packed array (figure 1(d)). The decay statistics for the arrayed geometry were similar to the isolated antenna. The other four antenna geometries exhibit a similar double exponential decay that is faster than the reference Rh800 in TEOS. The shortened excited state lifetime provides less opportunity for the molecules to photobleach, and thus the photostability of the system is increased [22, 49].

The polarization of the EF is measured in a transmission configuration to separate the polarization of the excitation source and the fluorescence signal. Fiber-coupled light from a HeNe laser illuminated the sample through the quartz substrate with linearly polarized 633 nm light through an inverted microscope with an objective lens (10× magnification, 0.25 NA). An upright microscope collected transmitted light though a second objective lens (20× magnification, 0.4 NA). The collected light passed through a 650 nm long-pass filter and a polarization analyzer and was measured in a spectrometer (Renishaw, inVia) (see figure 5(a)). A series of 25 spectra were collected, corresponding to a 360° rotation of the polarization analyzer. Measurements are presented comparing G2, G4 and G5 along with a reference taken away from the antenna arrays.

The enhancement and spectral shape of the fluorescence signal show a strong correlation with polarization. For light polarized along the primary antenna axis (X-direction, figure 5(b)), the fluorescence shows significant enhancement compared with the reference signal; each geometry shows distinct EF spectra based upon the LSPR mode which are similar to those in figure 2(b) (the long-pass filter used for figure 5 is different than that used for figure 2, so the features are a little different, especially for wavelengths below 700 nm). For Y-polarized light (figure 5(c)), we see that the shapes of the emission spectra from the different antenna geometries are similar to each other as well as to the reference spectrum of Rh800 away from any antenna interactions. This similarity in spectral shape, along with the weak enhancement factor, indicates that there is not much interaction between the antenna's primary LSPR mode and Rh800 for Y-polarized light. The fact that there is an enhancement for Y-polarized light but no change in the spectral shape compared with the reference signal points toward an enhancement of the local intensity of the excitation light (633 nm) by the nanoantenna arrays and thus an enhancement in absorption by the Rh800 dye. For Y-polarized light, the enhancement factors for G2, G4 and G5 are 6.0, 3.3 and 3.6, respectively. Qualitatively, and with reference to figure 2(d), this makes sense—the absorption enhancement at the excitation wavelength (633 nm) with the LSPR of G2 is greater than that of G4 and G5.

The mean intensity value ($I(P_\theta)$) for each polarization position is calculated by averaging over the fluorescence spectrum. This is plotted as a function of polarization angle in figure 5(d) for the four measurement sets. The fluorescence from a reference region on the sample shows a slight polarization in the X-direction. Compared with the reference emission, the nanoantenna-influenced emission is highly polarized. The polarization ratio $I(P_{180})/I(P_{90})$ for G2, G4 and G5 is calculated to be 6.5, 8.5 and 4.3, respectively, whereas the reference shows a ratio of only 1.2. The wavelength-averaged enhancement factor is calculated as $(I_{EF} - I_b)/(I_F - I_b)$,

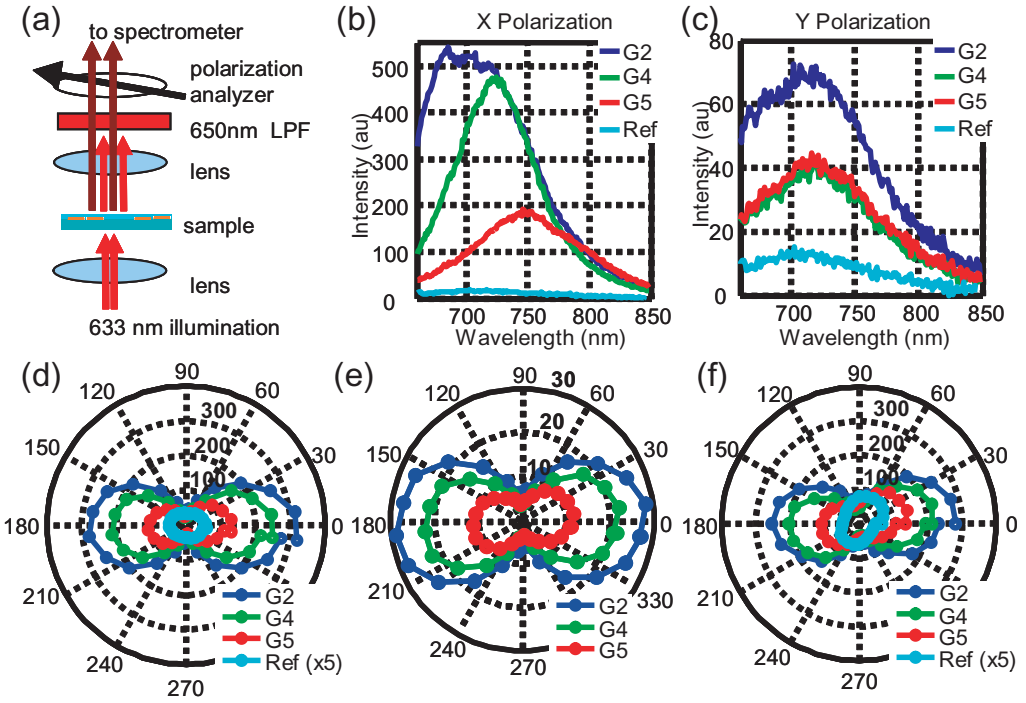

Figure 5. Polarization of fluorescence emission. (a) Measurement schematic. (b) Fluorescence spectra for *X*-polarized light corresponding to complete measurement shown in (d). (c) Same as (b) but for *Y*-polarized light. (d) Polar plot of enhanced emission compared with fluorescence emission away from the nanoantennae (wavelength integrated over emission range). (e) Polar plot of enhancement factor for the measurements shown in (d). (f) Similar measurement to (d) but for a different polarization of the excitation light.

where I_{EF} is the EF signal, I_F is the reference fluorescence signal and I_b is the instrumentation background signal. This is plotted in figure 5(e) and shows the same polarization tendencies as the EF. The fluorescence intensity of the last measurement point is slightly lower than the first measurement point due to photobleaching (figure 5(d)), but this effect disappears when the data are normalized to the enhancement factor (figure 5(e)). Another set of measurements were taken with the reference fluorescence exhibiting a polarization angle of approximately 60°. A polar plot of the averaged fluorescence is shown in figure 5(f), where the reference polarization is compared with the enhanced emission polarization. The EF signal redirects the polarization of the initial signal toward the primary antenna axis. G2 and G4 show higher fluorescence enhancement and rotate the fluorescence polarization more than G5, which has a weaker interaction with the dye. The redirection and polarization-selective enhancement of the fluorescence polarization is indicative of the plasmon mode of the antenna system and shows the nanoantenna's ability to control the emission of the dye placed around the nanoantenna. The polarization dependence of the enhanced emission has been discussed previously for both dimer [13, 25] and single [36]–[39] particle antenna systems. These drastic changes in emission polarization point toward the system's overall antenna-like nature in radiating near-field energy out into the far-field [50]–[52].

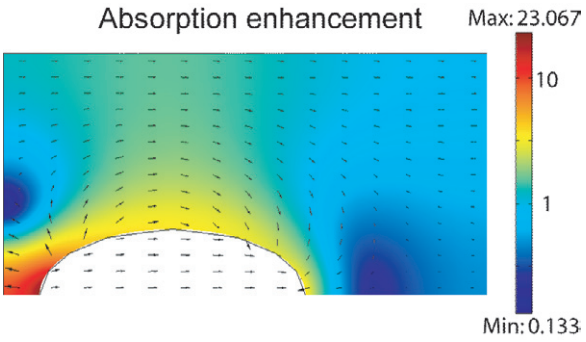

Figure 6. Enhancement map of the Rh800/TEOS layer absorption for G1 array at 630 nm; a cross section is taken 20 nm above the substrate (a quarter of the unit is shown due to symmetry). Arrows represent electric field vectors in log scale.

When a sample is illuminated with polarized light, those molecules with absorption transitions aligned parallel to the electric field have the highest probability of excitation. The probability of absorption is proportional to $\cos^2\theta$, where θ is the angle between the absorption dipole and the polarization. Hence, excitation with polarized light results in a population of excited molecules that are partially oriented along the light polarization axis. If the absorption and emission dipoles are collinear, the intensity of the emission polarized perpendicular to the excitation polarization is 1/3 that of the intensity for the parallel polarization [47]. This ratio can be affected by the angle between the absorption and emission dipoles. In the presence of the anisotropic antenna, there are two mechanisms for changes in the anisotropy of the fluorescence polarization. The first mechanism is illustrated in figure 6, which shows the distribution of the absorption enhancement for the Rh800/TEOS layer in the G1 array. One can see that the highest density of emitters with a preferential polarization parallel to the polarization of the excitation light (along the long axis here) occurs in the gap. Not only will these emitters be the most efficient in exciting the plasmon modes of the antenna, but they will also provide an additional factor for polarization anisotropy in the out-coupling of the fluorescence.

The out-coupled emission beam is formed by both direct dye emission and scattered emission via excited plasmon modes. The angular distribution of the emission can be directional [53, 54]. A manifestation of this directionality has been observed in our experiments. The enhancement ratio for two 50× objectives with NA = 0.45 and NA = 0.7 is about 1.5 for the G2 sample. Taking into account that the spectrally averaged enhancement for the first objective with an acceptance angle of $\theta_1 = 27^\circ$ is $K_1 = 30$, the enhancement ratio 1.5 indicates that for the second objective ($\theta_2 = 44^\circ$) the enhancement is $K_2 = 20$. One can estimate an average enhancement for a hemisphere assuming the emission intensity per solid angle is uniform for the dye/TEOS layer and has a smooth angular dependence for emission with the nanoantennae array. Note that only emission in the solid angle determined by the total internal reflection angle can go outside the dielectric layer. This means that the averaging over the hemisphere should be made inside the layer to take into account the entire emission. The acceptance angles for our objectives correspond to $\beta_1 = 18^\circ$ and $\beta_2 = 29^\circ$ inside the layer with a TEOS refractive index of 1.45. The first objective collects emission from a solid angle of about $\alpha_1 = 2\pi(1 - \cos\beta_1) = 0.3$, and the second from a solid angle of $\alpha_2 = 0.8$ inside the

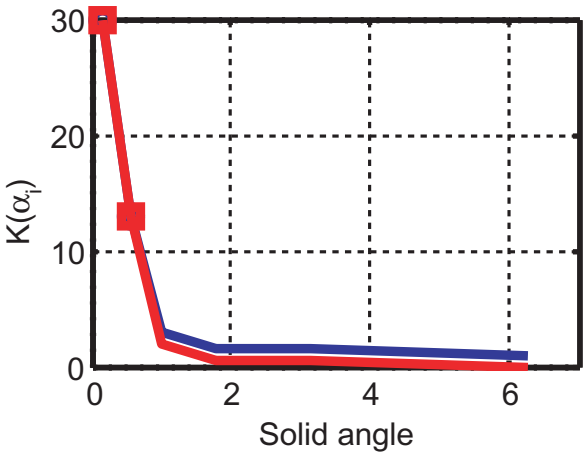

Figure 7. Fluorescence enhancement per unit solid angle versus objective acceptance solid angle inside the Rh800/TEOS layer. Blue—implies the assumption of an enhancement of about 1 at the larger solid angles. Red—using the assumption of zero enhancement at the larger solid angles.

layer. A simple proportion, $K_1\alpha_1 + K_{12}(\alpha_2 - \alpha_1) = K_2\alpha_2$ then leads to the enhancement factor $K_{12} = K_1/2.3$ in the solid angle $\alpha_2 - \alpha_1$. This dependence of the enhancement per unit solid angle versus solid angle is plotted in figure 7. The first two points in the figure are experimental, whereas all others are approximated implying a smooth dependence going to 1 (when there is no enhancement, upper plot) or to 0 (when everything is quenched, lower plot). The directionality effect does not contribute to the fluorescence signal averaged over a hemisphere of solid angles. Therefore, by estimating the average over a hemisphere, we can extract the contribution of excitation enhancement and quantum yield enhancement. The average enhancement $K_{2\pi}$ can be estimated from $2\pi K_{2\pi} = K_1\alpha_1 + K_{12}(\alpha_2 - \alpha_1) + \cdots + K_{nn-1}(\alpha_n - \alpha_{n-1})$. Using just the two first terms would give 2.5 for the average enhancement. If one applies a more realistic, smooth dependence as is shown in figure 7, the average enhancement $K_{2\pi}$ is about 3 or 4 depending on whether the upper or lower plot is selected. This estimate gives a factor of 2 for the lower bound of the quantum yield enhancement since the absorption enhancement is about 1.5–1.7.

In general, the measured fluorescence lifetime is defined as $\tau_o = (\Gamma_r + \gamma_{nr})^{-1}$ with a radiative decay rate Γ_r and a nonradiative decay rate γ_{nr}. The quantum yield is defined as $Q_o = \Gamma_r/(\Gamma_r + \gamma_{nr})$. Obviously $\Gamma_r \ll \gamma_{nr}$ if $Q_o \ll 1$, which is the case for Rh800 in a TEOS film. It follows from these formulae and the experimental result of a factor of three decrease in lifetime that the radiative decay rate is increased approximately by a factor of 6 and the nonradiative by a factor of 3 in the antenna–dye system.

In summary, we have studied the electric field enhancements afforded by the dimer nanoantenna configuration and how they can be exploited for enhancing the emission of a localized fluorescent dye. Gold elliptical dimers form the basis for optical nanoantennae that are tunable in the visible and near-infrared as a function of geometry, gap and host material choice. Emission and absorption of dye molecules (Rh800) are coupled to the nanoantenna system, and the nanoantenna system selectively enhances the fluorescence emission depending upon overlap of the plasmon resonance and the excitation wavelength and emission band.

Simulations show that the electric field intensity is highly localized around the edges of the elliptical nanoantennae with the maximum intensity in the antenna gap; as the antenna gap is

decreased, the average field intensity localized around the optical nanoantenna increases. When a fluorescent dye embedded in a host dielectric matrix is placed around the antenna array, it interacts with the dipolar plasmon mode of the nanoantennae, and EF is observed. The level of fluorescence enhancement depends on the spectral overlap between the LSPR mode and the dye absorption and emission along with the local field enhancement properties of the nanoantennae. As the antenna gap is decreased, an increase in fluorescence emission is observed. When the dye interacts with the nanoantennae, a reduced fluorescence lifetime is observed. The sample region with nanoantennae shows a double exponential decay when fitting the fluorescence lifetimes, indicating that molecules interacting with the nanoantennae exhibit a shorter decay time. With a dielectric thickness of 85 nm, there are also molecules that do not interact much with the antennae and exhibit a decay time similar to the reference signal measured away from any antennae. A strong emission directionality effect has been observed by varying the acceptance angle of the collection objective while maintaining the same magnification. In a representative sample, the spectrally averaged fluorescence signal collected by a 50× magnification objective with NA = 0.45 is increased by factor of 30 due to the presence of the Au nanoantenna array. In part, the observed enhancement is a result of the increased absorption at the excitation wavelength, giving an average factor of about 1.5–1.7 over the dye film volume (figure 2(d)). An estimate for a hemisphere-averaged enhancement leads to a quantum yield enhancement lower bound of about 2. The remaining contribution (roughly, by a factor of 10) to the observed 30-fold spectrally averaged enhancement originates from the antenna-induced directionality of emission. The quantum yield for Rh800 in a TEOS matrix is measured to be about $Q \approx 0.03$ and is much lower than the value in ethanol (0.21). Fluorescence lifetime (τ) measurements show that the excitation of the dye interacting with the nanoantenna decays at a rate three times faster than dye away from the nanoantenna. This lifetime decrease is mainly due to a 3-fold increase in the nonradiative decay rate γ_{nr}. Consequently, the radiative decay rate $\Gamma_{\mathrm{r}} = Q/\tau$ is increased by a factor of about 6. The plasmon-enhanced emission shows strong polarization preferences, forcing fluorophore emission toward the X-axis of the antenna geometry. Emission polarized along the Y-axis exhibits significantly less enhancement, and the spectral shape for the emission from the nanoantennae is the same for all geometries along with the reference emission.

We have studied a nanoantenna–emitter system that can be tailored to suit the needs of device designers. The ability to engineer the emission properties of a nanoantenna–emitter system will prove useful for future device applications.

Acknowledgments

This material is based upon work supported in part by the US Army Research Office under contract/grant number 50372-CH-MUR, ARO-STTR award W911NF-07-C-0008, NSF-PREM-DMR-0611430, NASA grant NCC-3-1035 and the Danish Research Agency NABIIT program (grant 2106-05-0033 (AB)). Useful discussions with Dr Noginov (Norfolk State University) and Mark Thoreson's kind assistance are also appreciated.

References

[1] Balanis C A 2005 *Antenna Theory: Analysis and Design* (Hoboken, NJ: Wiley)
[2] Novotny L 2007 *Phys. Rev. Lett.* **98** 266802
[3] Muhlschlegel P, Eisler H J, Martin O J F, Hecht B and Pohl D W 2005 *Science* **308** 1607

[4] Hecht B, Muhlschlegel P, Farahani J N, Eisler H-J, Pohl D W, Martin O J F and Biagioni P 2006 *Chimia* **60** 765
[5] Rechberger W, Hohenau A, Keitner A, Krenn J R, Lamprecht B and Aussenegg F R 2003 *Opt. Commun.* **220** 137
[6] Su K H, Wei Q H, Zheng X, Mock J J, Smith D R and Schultz S 2003 *Nano Lett.* **3** 1087
[7] Atay T, Song J-H and Nurmikko A V 2004 *Nano Lett.* **4** 1627
[8] Fromm D P, Sundaramurthy A, Schuck P J, Kino G and Moerner W E 2004 *Nano Lett.* **4** 957
[9] Jain P K, Huang W and El-Sayed M A 2007 *Nano Lett.* **7** 2080
[10] Sundaramurthy A, Crozier K B, Kino G S, Fromm D P, Schuck P J and Moerner W E 2005 *Phys. Rev.* B **72** 165409
[11] Farahani J N, Pohl D W, Eisler H-J and Hecht B 2005 *Phys. Rev. Lett.* **95** 017402
[12] Cubukcu E, Kort E A, Crozier K B and Capasso F 2006 *Appl. Phys. Lett.* **89** 093120
[13] Bek A, Jansen R, Ringler M, Mayilo S, Klar T A and Feldmann J 2008 *Nano Lett.* **8** 485
[14] Liu Z, Boltasseva A, Pedersen R H, Bakker R M, Kildishev A V, Drachev V P and Shalaev V M 2008 *Metamaterials* **2** 45
[15] Muskens O L, Giannini V, Sanchez-Gil J A and Gomez Rivas J 2007 *Opt. Express* **15** 17736
[16] Danckwerts M and Novotny L 2007 *Phys. Rev. Lett.* **98** 026104
[17] Bakker R M, Boltasseva A, Liu Z, Pedersen R H, Gresillon S, Kildishev A V, Drachev V P and Shalaev V M 2007 *Opt. Express* **15** 13682
[18] Merlein J, Kahl M, Zuschlag A, Sell A, Halm A, Boneberg J, Leiderer P, Leitenstorfer A and Bratschitsch R 2008 *Nat. Photonics* **2** 230
[19] Olk P, Renger J, Wenzel M T and Eng L M 2008 *Nano Lett.* **8** 1174
[20] Muskens O L, Giannini V, Sanchez-Gil J A and Gomez Rivas J 2007 *Nano Lett.* **7** 2871
[21] Muskens O L and Gomez Rivas J 2008 *Mater. Sci. Eng.* B **149** 216
[22] Zhang J, Fu Y, Chowdhury M H and Lakowicz J R 2007 *Nano Lett.* **7** 2101
[23] Bakker R M, Yuan H-K, Liu Z, Drachev V P, Kildishev A V, Shalaev V M, Pedersen R H, Gresillon S and Boltasseva A 2008 *Appl. Phys. Lett.* **92** 043101
[24] Rogobete L, Kaminski F, Agio M and Sandoghdar V 2007 *Opt. Lett.* **32** 1623
[25] Liaw J-W 2007 *Japan. J. Appl. Phys.* **46** 5373
[26] Talley C E, Jackson J B, Oubre C, Grady N K, Hollars C W, Lane S M, Huser T R, Nordlander P and Halas N J 2005 *Nano Lett.* **5** 1569
[27] Imura K, Okamoto H, Hossain M K and Kitajima M 2006 *Nano Lett.* **6** 2173
[28] Tang L, Kocabas S E, Latif S, Okyay A K, Ly-Gagnon D-S, Saraswat K C and Miller D A B 2008 *Nat. Photonics* **2** 226
[29] Corrigan T D, Guo S-H, Phaneuf R J and Szmacinski H 2005 *J. Fluorescence* **15** 777
[30] Song J-H, Atay T, Shi S, Urabe H and Nurmikko A V 2005 *Nano Lett.* **5** 1557
[31] Anger P, Bharadwaj P and Novotny L 2006 *Phys. Rev. Lett.* **96** 113002
[32] Kuhn S, Hakanson U, Rogobete L and Sandoghdar V 2006 *Phys. Rev. Lett.* **97** 017402
[33] Biteen J S, Lewis N S, Atwater H A, Mertens H and Polman A 2006 *Appl. Phys. Lett.* **88** 131109
[34] Chen Y, Munechika K and Ginger D S 2007 *Nano Lett.* **7** 690
[35] Kuehn S, Mori G, Agio M and Sandoghdar V 2008 *Mol. Phys.* **106** 893
[36] Mertens H and Polman A 2006 *Appl. Phys. Lett.* **89** 211107
[37] Mertens H, Biteen J S, Atwater H A and Polman A 2006 *Nano Lett.* **6** 2622
[38] Taminiau T H, Moerland R J, Segerink F B, Kuipers L and van Hulst N F 2007 *Nano Lett.* **7** 28
[39] Taminiau T H, Stefani F D, Segerink F B and Van Hulst N F 2008 *Nat. Photonics* **2** 234
[40] Moerland R J, Taminiau T H, Novotny L, van Hulst N F and Kuipers L 2008 *Nano Lett.* **8** 606
[41] Kreibig U and Vollmer M 1995 *Optical Properties of Metal Clusters* (Berlin: Springer)
[42] Gersten J and Nitzan A 1981 *J. Chem. Phys.* **75** 1139
[43] Ruppin R 1982 *J. Chem. Phys.* **76** 1681

[44] Khurgin J B, Sun G and Soref R A 2008 *Appl. Phys. Lett.* **93** 021120
[45] Sun G, Khurgin J B and Soref R A 2008 *J. Opt. Soc. Am.* B **25** 1748
[46] Bachteler B, Drexhage K H, Arden-Jacob J, Han K T, Kollner M, Muller R, Sauer M, Seeger S and Wolfrum J 1994 *J. Lumin.* **62** 101
[47] Lakowicz J R 2006 *Principles of Fluorescence Spectroscopy* (New York: Springer)
[48] Wahl M, Koberling F, Patting M, Rahn H and Erdmann R 2004 *Curr. Pharmaceutical Biotechnol.* **5** 299
[49] Vasiev K, Stefani F D, Jacobsen V, Knoll W and Kreiter M 2004 *J. Chem. Phys.* **120** 6701
[50] Li J, Salandrino A and Engheta N 2007 *Phys. Rev.* B **76** 245403
[51] Hofmann H F, Kosako T and Kadoya Y 2007 *New J. Phys.* **9** 217
[52] Taminiau T H, Stefani F D and Van Hulst N F 2008 *Opt. Express* **16** 10858
[53] Matthews D R, Summers H D, Njoh K, Chappell S, Errington R and Smith P 2007 *Opt. Express* **15** 3478
[54] Martin-Mareno L, Garcia-Vidal F J, Lezec L J, Degiron A and Ebessen T W 2003 *Phys. Rev. Lett.* **90** 167401